

Structural transition in epitaxial Co-Cr superlattices

W. Vavra

Department of Physics, The University of Michigan, Ann Arbor, Michigan 48109

D. Barlett

Department of Physics and Applied Physics Program, The University of Michigan, Ann Arbor, Michigan 48109

S. Elagoz, C. Uher, and Roy Clarke

Department of Physics, The University of Michigan, Ann Arbor, Michigan 48109

(Received 29 October 1992)

Using a real-time reflection high-energy electron diffraction analysis technique, we show that the epitaxial growth of Co-Cr superlattices incorporates coherent close-packed Cr layers up to a thickness of 6 Å. Beyond this thickness there is an abrupt structural transition to bcc (110) Cr in the classic Nishiyama-Wasserman and Kurdjumov-Sachs orientations. Magnetization and magnetoresistance results indicate that interlayer coupling is very weak, which we attribute to the altered crystal structure in the Cr layers.

The fascinating array of magnetic coupling phenomena in Fe-Cr thin films and multilayers has led to a resurgence of activity in itinerant electron magnetism. This began with the discovery by Grünberg^{1,2} that Fe films couple together antiferromagnetically if separated by a thin (≈ 10 Å) Cr layer. Soon after this it was dramatically demonstrated that this coupling resulted in "giant" magnetoresistance effects.^{3,4} More recently, the sign and strength of the coupling were shown to oscillate as the thickness of the Cr interlayer is varied and it was found that the period of oscillation is dependent upon the structural quality of the film.⁵⁻⁷ In light of these phenomena in the Fe-Cr system it is natural to ask if, and under what conditions, they would occur if Fe is replaced by Co. The complication is that Co prefers an hcp structure instead of the bcc form of Fe and Cr.

In this paper we report the results of a time-resolved, quantitative reflection high-energy electron diffraction (RHEED) study on the growth of Co-Cr superlattices. Using a newly developed charge coupled device (CCD)-based detection and analysis system,⁸ lattice spacing and domain size were recorded simultaneously as a function of film thickness. The data reveal an abrupt transition of Cr from a *close-packed* arrangement, for thicknesses up to ≈ 6 Å, to both Kurdjumov-Sachs and Nishiyama-Wasserman bcc orientations. In contrast to the Fe-Cr system and sputtered Co-Cr multilayers,⁵ we find little evidence for interlayer coupling, which we attribute to the altered crystal (and hence electronic) structure of the Cr layers.

Samples were grown on (110) GaAs substrates in a Vacuum Generators V80 molecular beam epitaxy chamber at $1-5 \times 10^{-9}$ mbar. Cr and Co were evaporated from electron beam hearths at rates that ranged from 0.35 to 0.5 Å/sec. Cr rates lower than this led to poor sample quality indicating that supersaturation growth conditions are beneficial. To establish a smooth (0001) Co surface on which to begin superlattice growth the following buffer layers were grown on the GaAs: first, 500

Å of (110) Ge, then 25 Å bcc Co, and finally 20 Å (111) Au. Superlattice bilayers consisting of $[20 \text{ Å Co}/x \text{ Å Cr}]$ with $x = 4, 6, 8, 10$, and 12 Å were then grown on the Au. Lastly, a protective 10 Å Au cap was deposited on the samples. The Ge was grown at 550°C, all metals at 50°C, and the total thickness of each superlattice is 1000 Å. X-ray photoemission showed sample contamination (e.g., oxygen and carbon) was less than the detectable limit ($< 2\%$).

Figure 1 shows an x-ray χ scan, in which the diffraction vector lies in the sample plane,⁹ for a $[20 \text{ Å Co}/4 \text{ Å Cr}]_{42}$ superlattice. The diffraction peaks with 60° symmetry indicate a highly coherent close-packed structure. A c^* scan [inset (b)], which probes the stacking of the layers,⁹ indicates the Co is (0001)-oriented hcp, and a low angle scan [inset (a)] shows well formed superlattice peaks. Although the Co is hcp, we use fcc notation to describe all surface directions. This is done to make comparisons with previous literature more straightforward, as well as to simplify the notation.

We now turn our attention to the RHEED images of Fig. 2. These are diffraction patterns from Co and Cr layers in the samples with 4 and 10 Å Cr thickness and the electron beam parallel to $\text{Co}\langle 110 \rangle$. One can see that the superlattice is well ordered for the sample with 4 Å Cr layers, but the RHEED pattern indicates a structural transition has occurred for the 10 Å Cr sample. Two separate regions of the RHEED patterns were monitored simultaneously during growth. These two regions are labeled "NW" and "KS" in Fig. 2, to be explained below. Note the same regions were scanned for all the superlattices, but these regions become visibly distinct only after the structural transition has occurred. Streak separation and width (lattice spacing and domain size) were measured in these two regions at a rate of 15 data points per Å during deposition. The same measurements were also performed along the other major azimuth, $\text{Co}\langle 112 \rangle$. Absolute values of lattice spacings are calibrated with respect to the Au buffer layer. Domain sizes (see Fig. 3

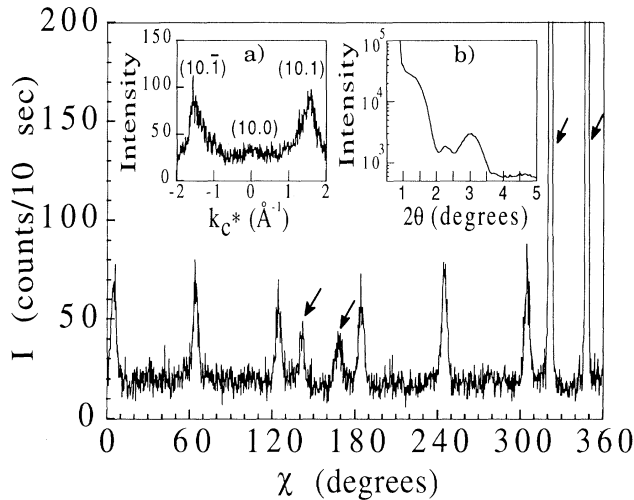


FIG. 1. X-ray χ scan for $[20 \text{ \AA Co}/4 \text{ \AA Cr}]_{42}$ superlattice, showing diffraction peaks with 60° symmetry. Inset (a): x-ray c^* scan indicating hcp stacking of Co layers. Inset (b): low-angle x-ray scan showing superlattice peaks. Arrows indicate GaAs (113) and (420) peaks.

insets) are lower limits and strictly speaking are the average in-plane structural coherence length perpendicular to the incident electron beam. The contribution to the widths from instrument broadening has been deconvolved from the data.

In Fig. 3(a) we have plotted lattice spacing versus

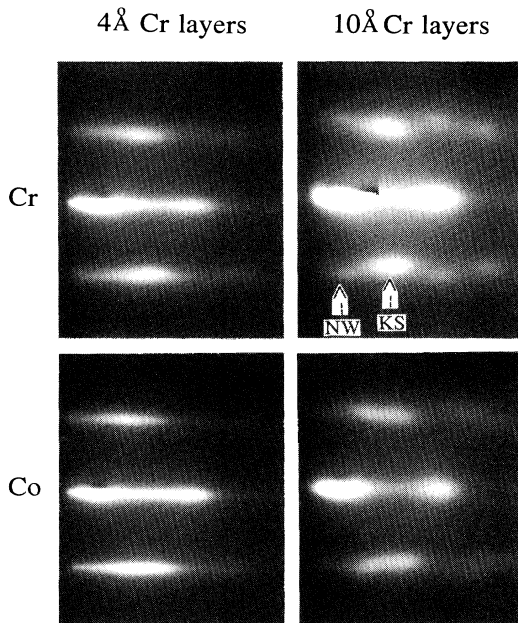


FIG. 2. Representative RHEED images along the $\text{Co}\langle 110 \rangle$ direction. Sharp RHEED streaks are seen for the Co and Cr layers of the $[20 \text{ \AA Co}/4 \text{ \AA Cr}]_{42}$ superlattice. In contrast, the Co and Cr layers of the $[20 \text{ \AA Co}/10 \text{ \AA Cr}]_{33}$ superlattice indicate a structural transition has occurred.

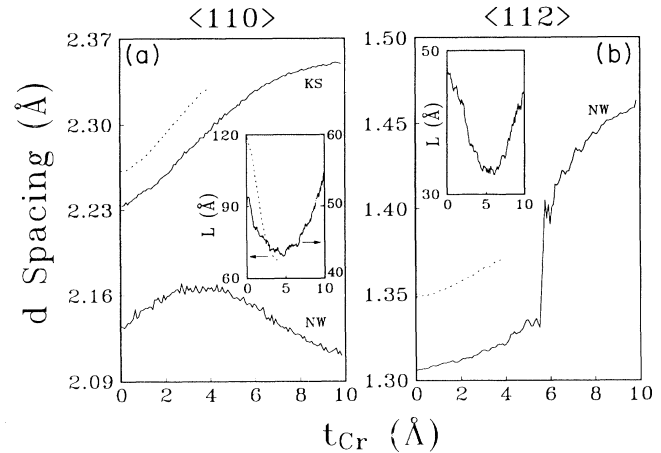


FIG. 3. (a) d spacing profiles during growth of the Cr layers shown in Fig. 2. The RHEED beam is parallel to $\text{Co}\langle 110 \rangle$, while the dashed and solid lines refer to the 4 \AA and 10 \AA Cr layers, respectively. (b) RHEED beam parallel to $\text{Co}\langle 112 \rangle$. Insets are domain size (L) profiles with arrows indicating the appropriate y axis. The x axes are the same scale as in the d spacing plots.

thickness of the same Cr layers shown in Fig. 2. Again, the RHEED beam is parallel to $\text{Co}\langle 110 \rangle$. First, we see that the epitaxial strain of the overlayer begins relaxing as soon as growth is started. Therefore, there is no critical thickness up to which true pseudomorphic growth occurs without the formation of misfit dislocations [Fig. 3(a) inset]. This is in contrast to strained-layer semiconductor growth,¹⁰ and is due in part to the isotropic nature of the metallic bond compared with the more directional semiconductor bond.

The most important feature in Fig. 3 is that the Cr d spacing initially *increases* along *both* azimuths during growth. We will show presently that this is inconsistent with bcc Cr growth. The 4 \AA Cr layers (dashed lines) show an increase in d spacing throughout the growth of the layer, whereas the 10 \AA Cr layers (solid lines) undergo uniform expansion only until $4\text{--}5 \text{ \AA}$ Cr thickness. Beyond this thickness the d spacing along $\text{Co}\langle 110 \rangle$ [Fig. 3(a)] reaches a maximum in the NW region, then begins decreasing. This maximum in d spacing coincides with a minimum in domain size [Fig. 3(a) inset]. In other words the misfit dislocation density increases with Cr thickness until there is a transition to a lower strain energy form of epitaxy, then the sample begins healing. Along $\text{Co}\langle 112 \rangle$ [Fig. 3(b)] the Cr transition is even more pronounced. At $4\text{--}6 \text{ \AA}$ an abrupt 15% change in the d spacing occurs. Correspondingly, the domain profile (inset) shows a deep minimum at this thickness and then the surface becomes more coherent. This again clearly shows evidence for a structural transition.

The analysis of the transition is based on extensive work found in the literature on bcc (110)/fcc (111) [or hcp (0001)] metal epitaxy. Enlightening theoretical predictions of the orientation and growth for this kind of heteroepitaxy have been performed by several authors.^{11–14} The results of these studies show that minima in the total overlayer free energy occur for orientations

such that the most densely packed rows are parallel. This is easily seen by considering the potential energy of a monolayer deposited on a substrate.¹⁴

$$U = \phi_0 + \sum_{\mathbf{G}} \sum_{\mathbf{G}'} \phi_{\mathbf{G}} \delta_{\mathbf{G}, \mathbf{G}'}$$

Here \mathbf{G} and \mathbf{G}' are the surface reciprocal lattice vectors (rlv's) of the substrate and overlayer, respectively, and $\phi_{\mathbf{G}}$ are unknown *negative* Fourier coefficients whose absolute values increase rapidly with decreasing $|\mathbf{G}|$. This expression shows that the total potential energy is lowered by matching overlayer and substrate rlv's, i.e., by atomic row matching. The lowest-energy configuration is where *all* rlv's match and the overlayer assumes the structure of the substrate. There is, however, an increase in strain energy as the thickness of this pseudomorphic layer increases. When these two competing terms offset each other there is a transition to the next lowest energy configuration. In this next configuration the overlayer takes its preferred (bulk) phase and aligns its *shortest* rlv's with those of the substrate, thus making the most densely packed rows of atoms parallel. These orientations correspond to the classic Kurdjumov-Sachs (KS) ($\text{Cr}\langle 111 \rangle \parallel \text{Co}\langle 110 \rangle$) and Nishiyama-Wasserman (NW) ($\text{Cr}\langle 001 \rangle \parallel \text{Co}\langle 110 \rangle$) orientations. The KS and NW orientations for Co-Cr are illustrated in Fig. 4, with row spacing mismatches of $(d^{\text{Cr}} - d^{\text{Co}})/d^{\text{Co}} = 8.5\%$ and -6.1% respectively.

Our d spacing data for the five samples are summarized in Fig. 5. The underlying (bulk) Co in-plane d spacings are also plotted for reference. Measured d spacings are taken from the top surface of individual layers, and these were typically averaged over 3–4 layers at various stages of growth for each superlattice. We emphasize that Fig. 5 is *not* a growth front profile as in Fig. 3, but is a plot of the average Cr layer d spacing for each of the superlattices. Figure 5 shows that after the transition

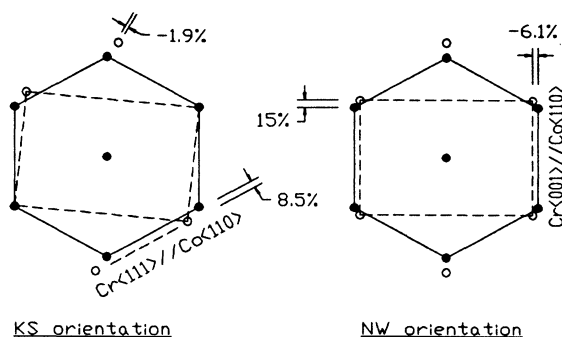


FIG. 4. Schematic diagram of bcc (110) Cr mesh (open circles and dashed line) on hcp (0001) Co mesh in the KS and NW orientations. As in the text, Co directions are given in fcc notation. Row spacing mismatches were determined using the bulk lattice constants $a(\text{Co}) = 2.507 \text{ \AA}$ and $a(\text{Cr}) = 2.884 \text{ \AA}$. We have also labeled the misfit along $\text{Co}\langle 112 \rangle$ for the two orientations: for KS, $\text{Cr}\langle 113 \rangle$ is within 0.5° of being parallel to $\text{Co}\langle 112 \rangle$ with a mismatch of -1.9% , and for NW, $\text{Cr}\langle 110 \rangle$ is parallel to $\text{Co}\langle 112 \rangle$ and the mismatch is 15% . Our measured strains along these directions are given in Figs. 3(b) and 5(b).

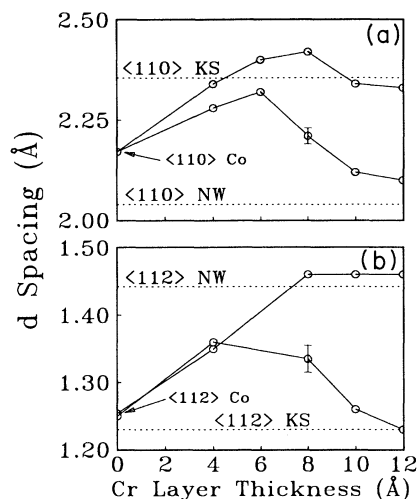


FIG. 5. Average Cr d spacings for the series of Co-Cr superlattices. Measured d spacings are taken from the top surface of individual layers and these were typically averaged over 3–4 layers at various stages of each superlattice. For reference, the underlying (bulk) Co (0001) d spacings are plotted at zero thickness. The dashed lines show the expected d spacings for bcc (110) Cr in the indicated orientations. In (a) the data suggest that the 4 Å and 6 Å Cr samples are in the KS orientation, however, the increase in d spacing along $\text{Co}\langle 112 \rangle$ is inconsistent with KS. Data along $\text{Co}\langle 112 \rangle$ were not recorded for the 6 Å Cr sample.

the measured d spacings for both directions approach those expected for the KS and NW orientations. In contrast, we see isomorphic Cr expansion for the 4 Å and 6 Å Cr samples, which is inconsistent with bcc growth in the NW or KS orientations. This isomorphic expansion, plus the strong 60° in-plane symmetry and large in-plane coherence length for these samples (from RHEED and x-ray analysis), indicates that the 4 Å and 6 Å Cr superlattices are strained coherently into the close-packed structure of the underlying Co.

Figure 6 shows the evolution of the Cr first-order

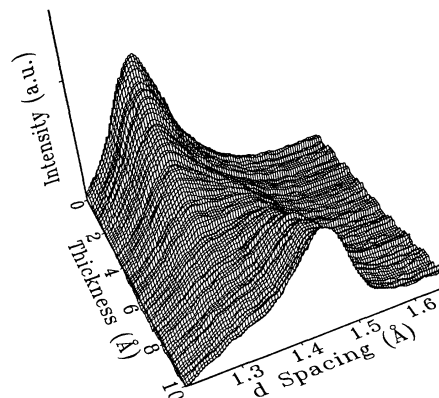


FIG. 6. Evolution of Cr RHEED streak along $\text{Co}\langle 112 \rangle$ during the growth of the fifth Cr layer in the $[\text{Co } 20 \text{ \AA} / 10 \text{ \AA} \text{ Cr}]_{33}$ superlattice. The plot shows the growth of 4–5 Å of close-packed Cr on (0001) Co, followed by a transition to bcc (110) Cr. The 15% change in d spacing and the final d spacing value are consistent with bcc (110) Cr in the NW orientation.

RHEED streak during the growth of a 10 Å Cr layer. The electron beam is along Co(112). Initially the Cr strains to the underlying close-packed Co d spacing, but an abrupt 15% change and a final d spacing value of 1.46 Å are indicative of bcc (110) Cr in the NW orientation (see Fig. 4). It is important to point out that we see diffraction from both orientations along a given azimuthal direction: hence the labeling "NW" region and "KS" region in the images of Fig. 2. This is due to the sixfold symmetry of the hcp (0001) surface allowing three equivalent alignments for a given orientation.

In summary, we have grown a series of epitaxial Co-Cr superlattices in which the first 5–6 Å of each Cr layer is close-packed. Beyond this thickness there is an abrupt transition to the Kurdjumov-Sachs and Nishiyama-Wasserman bcc orientations. In contrast to Fe-Cr superlattices we find very weak coupling across the Cr layers. Magnetoresistance values (at 5 K) of only 0.4, 0.4, 0.2,

0.1, and 0.4 % for the samples with 4, 6, 8, 10, and 12 Å Cr layers rule out antiferromagnetic coupling, while remanent magnetizations of 0.2, 0.2, 0.3, 0.3, and 0.4 % could result from weak ferromagnetic coupling. Given the altered crystal structure of the Cr it is reasonable to expect its electronic structure to be significantly different than bulk Cr. This is also expected based on band-structure calculations of fcc (Ref. 15) and hcp (Ref. 16) Cr which predict a density of states at the Fermi energy roughly three times higher than for bcc Cr. These changes in the electronic structure can inhibit the formation of spin-density waves which have been identified with the interlayer coupling in Fe-Cr structures.¹⁷

We thank Peter Levy for helpful discussions. This work was supported by Office of Naval Research Grant No. N00014-92-J-1335.

¹P. Grünberg, J. Appl. Phys. **57**, 3673 (1985).

²P. Grünberg, R. Schreiber, Y. Pang, M. B. Brodsky, and H. Sowers, Phys. Rev. Lett. **57**, 2442 (1986).

³M. N. Baibich, J. M. Broto, A. Fert, F. Nguyen Van Dau, F. Petroff, P. Eitenne, G. Creuzet, A. Friederich, and J. Chazelas, Phys. Rev. Lett. **61**, 2472 (1988).

⁴G. Binasch, P. Grünberg, F. Saurenbach, and W. Zinn, Phys. Rev. B **39**, 4828 (1989).

⁵S. S. P. Parkin, N. More, and K. P. Roche, Phys. Rev. Lett. **64**, 2304 (1990).

⁶J. Unguris, R. J. Celotta, and D. T. Pierce, Phys. Rev. Lett. **67**, 140 (1991).

⁷S. T. Purcell, W. Folkerts, M. T. Johnson, N. W. E. McGee, K. Jager, J. aan de Stegge, W. B. Zeper, W. Hoving, and P. Grünberg, Phys. Rev. Lett. **67**, 903 (1991).

⁸D. Bartlett, C. W. Snyder, B. G. Orr, and Roy Clarke, Rev. Sci. Instrum. **62**, 1263 (1991); marketed as Model KSA 300 by k-

space Associates Inc.

⁹F. J. Lamelas, C. H. Lee, Hui He, W. Vavra, and Roy Clarke, Phys. Rev. B **40**, 5837 (1989).

¹⁰C. W. Snyder, D. Barlett, B. G. Orr, P. K. Bhattacharya, and J. Singh, J. Vac. Sci. Technol. B **9**, 2189 (1991).

¹¹L. A. Bruce and H. Jaeger, Philos. Mag. A **38**, 223 (1978).

¹²E. Bauer and J. H. van der Merwe, Phys. Rev. B **33**, 3657 (1986).

¹³R. Ramirez, A. Rahman, and I. K. Schuller, Phys. Rev. B **30**, 6208 (1984).

¹⁴S. Stoyanov, Surf. Sci. **172**, 198 (1986).

¹⁵Jian-hua Xu, A. J. Freeman, T. Jarlborg, and M. B. Brodsky, Phys. Rev. B **29**, 1250 (1984).

¹⁶D. A. Papaconstantopoulos, J. L. Fry, and N. E. Brener, Phys. Rev. B **39**, 2526 (1989).

¹⁷Y. Wang, P. M. Levy, and J. L. Fry, Phys. Rev. Lett. **65**, 2732 (1990).

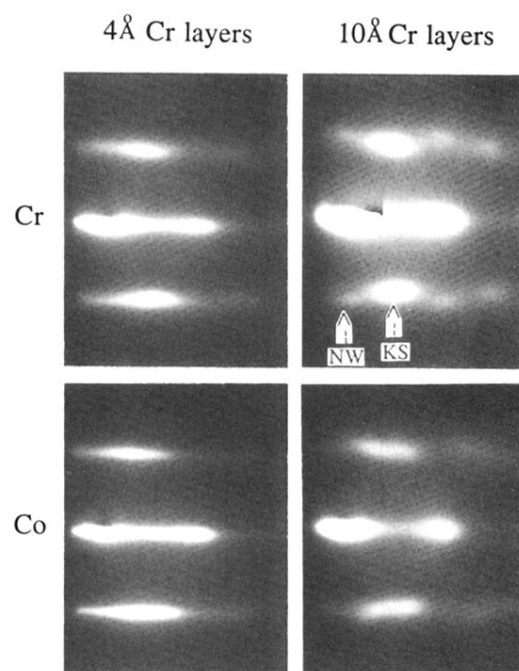


FIG. 2. Representative RHEED images along the $\text{Co}\langle 110 \rangle$ direction. Sharp RHEED streaks are seen for the Co and Cr layers of the $[20 \text{ Å Co} / 4 \text{ Å Cr}]_{42}$ superlattice. In contrast, the Co and Cr layers of the $[20 \text{ Å Co} / 10 \text{ Å Cr}]_{33}$ superlattice indicate a structural transition has occurred.